THE JOURNAL OF PHYSICAL CHEMISTRY C
A JOURNAL OF THE AMERICAN CHEMICAL SOCIETY

pubs.acs.org/JPCC Article

# Water Diffusion Effects at Gold−Graphene Interfaces Supporting Surface Plasmon Polaritons

Quaid Zaman, Tahir, Fernando Lazaro Freire, Jr., Ivan Shtepliuk, Andre N. Barbosa, Marcelo E. H. Maia da Costa, Cesar Augusto Diaz Mendoza, Jefferson F. D. F Araujo, Guilherme C. Concas, Marco Cremona, Zubair Ahmed, Omar Ginoble Pandoli, Ricardo Q. Aucelio, Victor Dmitriev, Karlo Q. da Costa, André Felipe S. Cruz, Gabriella Fibbi, Anna Laurenzana, Francesca Margheri, Anastasia Chillà, Francesca Scavone, Elena Frediani, Rajwali Khan, Nicola Daldosso, Elena Chistè, Gino Mariotto, Evelyn C. S. Santos, and Tommaso Del Rosso*

Cite This: *J. Phys. Chem. C* 2022, 126, 13905−13919 Read Online



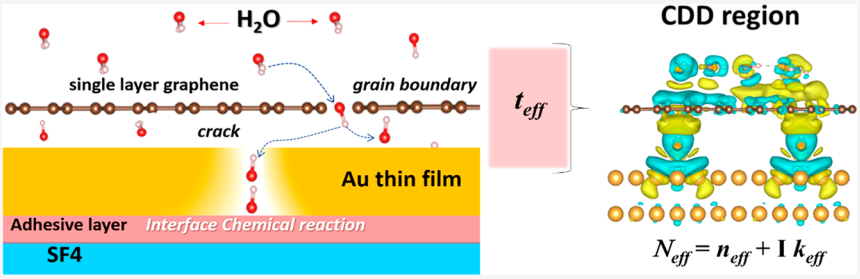


**ABSTRACT:** We present a detailed investigation on the effects of water diffusion at the different interfaces of gold−graphene plasmonic sensors on the propagation of the supported surface plasmon polaritons (SPPs). The substrate/metal interfacial chemical reactions are investigated by monitoring the full width at half-maximum of the SPR reflectivity curve. Although protection by single-layer graphene (SLG) grown by chemical vapor deposition inhibits the chemical reactions happening at the metal−dielectric interfaces, SPR experimental results confirm that water diffusion paths through the borders of graphene domains are still present into the plasmonic sensors. Density functional theory calculations show that the doping level of SLG after the transfer on gold as well as interfacial charge transfer can be tuned in the presence of water molecules. On these bases, we propose a simplified effective medium approach for heterogeneous metal−carbon interfaces, where the interaction between the surface atomic layers of the gold thin film, water molecules, and the SLG induces the creation of an extended charge density difference region crossing the Au/$H_2O$/SLG/$H_2O$ heterointerface. The latter is modeled as an ultrathin effective medium with a thickness and extraordinary optical susceptivity and conductivity that are different from those of the free-standing graphene. In this context, the extraordinary refractive index and thickness of the graphene−gold effective medium are measured in the near-infrared on the low-damping SPR platforms by applying the two-medium SPR method. The results are coherent with graphene n-doping in water environment, showing that the optically excited electrons along the extraordinary axis have a substantial bonding character and that the enhancement of the sensitivity of the gold−graphene plasmonic sensors is not related to a shift in the plasma frequency of the metal layer but to the changes in the extraordinary polarizability of graphene. The research highlights the importance of the SLG−substrate and SLG−environment interactions in graphene-protected plasmonics and optoelectronics.

## 1. INTRODUCTION

Surface plasmon polaritons (SPPs) are electromagnetic surface waves, excited across metal−dielectric interfaces when a p-polarized light is coupled with the collective oscillations of the free electrons in metals.[1] Surface plasmon resonance (SPR) spectroscopy is performed in attenuated total reflection (ATR) conditions, most frequently in the so-called Kretschmann configuration.[1] In the ATR regime, a minimum of the reflectivity can be observed at a particular angle called the SPR angle, which is highly dependent on the refractive index of the media on the top side of the metal.

**Received:** April 24, 2022
**Revised:** July 27, 2022
**Published:** August 3, 2022

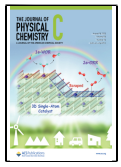







https://doi.org/10.1021/acs.jpcc.2c02841
*J. Phys. Chem. C* 2022, 126, 13905−13919

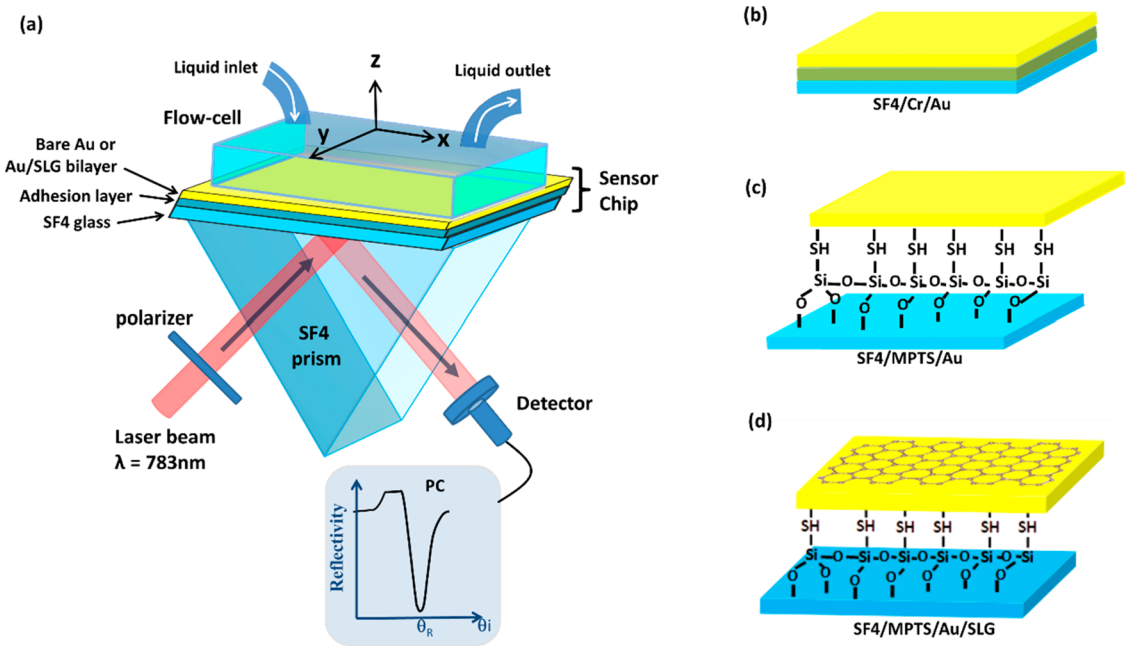


**Figure 1.** (a) Schematic representation of proposed SPR sensors in Krestschmann configuration comprising the prism, sensor chip, and flow-cell for liquid injection. Right: Sensor chips based on gold thin film with different metal−dielectric interfaces. Bare gold thin film with (b) Cr or (c) MPTS as adhesion layers. (d) Gold−graphene SPR sensor, with MPTS adhesion layer and SLG deposited over the gold film.

Comprehensive theoretical and experimental studies suggested that the enhancement in sensitivity and chemical stability of conventional SPR optical sensors strongly depends on (i) the choice of metal thin film,[2] (ii) the adhesion layer between metal film and dielectric substrate,[3] and (iii) the incorporation of a protective and inert coating layer such as graphene onto SPR sensing platforms.[4]

Although gold (Au)-based sensors with a broader SPR curve may yield a lower sensitivity than silver (Ag),[5] the majority of plasmonics biosensors use a gold film to support the plasma wave because of its excellent chemical stability toward oxidation, in both air or water environments.[6]

Another factor that plays a crucial role in the sensitivity of SPR sensors is the choice of the metal−glass ligand, which may significantly alter the SPP damping.[7] To enhance adhesion, chromium (Cr) or titanium (Ti) are generally used as a metallic ultrathin intermediate layer (2−5 nm) between gold and glass substrates.[8] However, the addition of these metallic layers provokes a severe chemical interface plasmon damping, caused by the partial oxidation of the adhesion metal during the thin-film deposition and its diffusion into the Au layers.[9−11]

In this context, also transparent molecular ligands have been experimentally investigated, generally presenting the best results in terms of stability and figure of merit (FOM) of the plasmonic nanostructures or devices.[3,10,12,13] (3-Mercaptopropyl) trimethoxysilane (MPTS) has been used by our group as an interface chemical bridge in plasmonic devices aiming to the characterization of thin films of organic materials,[14−17] but no study is available at the moment concerning the influence of this metal−organic interface on the stability, sensitivity, and FOM of SPR sensors based on SPPs.

Another important parameter often underestimated in plasmonics-related literature is moisture. The latter is considered traditionally as one of the most critical factors inducing instability in the optical properties of multilayer metal−dielectric thin films[18,19] because of the amplification of intrinsic stresses after fabrication, inducing cracks and chemical reactions at the crack-tip, leading eventually to delamination.[19−22] This phenomenon is critical, for example, in all the thin-film interconnected structures present in microelectromechanical system (MEMS) devices, microelectronics, or optical filters.[19,20,22,23] Moreover, it is known that in metal−glass interfaces the expansion and evolution of the cracks depend strongly on the humidity conditions.[20,24−26] In this context, it is somehow surprising that in the literature is still missing a study of the modification of the optical and morphological properties of glass/adhesive layer/Au interface due to the eventual diffusion of water molecules across the plasmonic thin film.

In the past decade, the modification of the external surface of the device in contact with the liquid environment has been used to enhance the stability and/or sensitivity of SPR sensors in the Kreschtmann configuration. Examples are the nanoparticle-amplified surface plasmon resonance (PA-SPR) spectroscopy[13,14,17] and graphene supported plasmonics, where a single-layer graphene (SLG) is transferred on gold thin films supporting SPPs.[27] In the latter case, it has been proposed that the enhancement in the sensitivity originates from the transfer of electrons from graphene to gold due to the difference in the Fermi energy of the two materials, with subsequent increase in the plasma frequency of the metal.[27,28] Although most of the SPR investigations on the gold−graphene planar interfaces coherently report the enhancement in the sensitivity[27,29,30] or stability[31] of the sensors, the experimental values of thickness and extraordinary optical constant of the SLG transferred over gold surfaces are highly scattered, and the reasons for this behavior are not deeply investigated, discussed, and understood.[31−33]

In the present research, we take into consideration the interaction of graphene with both the liquid environment and the substrate, including the possibility of the intercalation of water molecules into the Au/SLG bilayer,[34] and propose it as


https://doi.org/10.1021/acs.jpcc.2c02841
J. Phys. Chem. C 2022, 126, 13905−13919

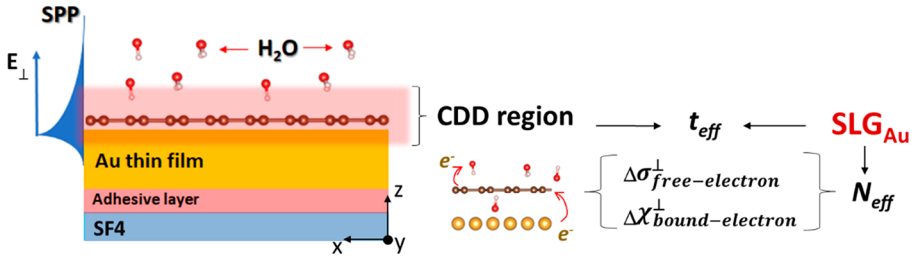


**Figure 2.** Scheme of the gold−graphene SPR sensor chip. The electron transfer defines the graphene−gold effective medium $SLG_{Au}$, the thin region across the Au/SLG/$H_2O$ interfaces with a net charge density difference (CDD), indicated in red. The evanescent electric field of the surface plasmon polariton (SPP) $\mathbf{E}_{\perp}$, represented in blue, is polarized along the *z*-axis perpendicular to the planar interfaces, so that the interaction and charge transfer between the carbon and gold atoms and water molecules affects only the extraordinary (⊥) optical susceptivity and conductivity of the $SLG_{Au}$. The *xyz* axes are represented at the bottom of the sensor chip.

one of the possible reasons leading to the spread of the experimental values found in the literature. We suppose that the interaction of the SLG with the environment and substrate defines a region surrounding the SLG where the charge density is altered by electron transfer[28] creating an ultrathin effective medium we define as $SLG_{Au}$, with an effective thickness and optical constants different from those of the suspended graphene.

We start by investigating by SPR spectroscopy and atomic force microscopy (AFM) the effects that water diffusion across bare plasmonic gold thin films has on the stability and sensitivity of the sensors. Furthermore, the effect of the SLG transfer is studied in terms of stability, sensitivity, and FOM of the gold−graphene plasmonic sensors in the near-infrared region.

DFT calculations are used to predict the charge transfer between the SLG and the gold thin film, showing that the kind of SLG doping is highly sensitive to the presence of water molecules interacting with the SLG. The results are subsequently linked to the determination of the effective thickness and extraordinary optical constant of the $SLG_{Au}$, in the frame of an effective medium optical approach and two-medium SPR technique.[35] We finally explain the results by the modification of the extraordinary optical susceptivity and/or conductivity of the SLG upon interaction with gold and water molecules, suggesting alternative routes to the interpretation of the enhancement of the sensitivity of the optical sensors based on gold−graphene interfaces in water.

**1.1. Experimental Scheme for SPR Spectroscopy.** A sketch of the proposed SPR sensors operating in the Krestschmann configuration is shown in Figure 1a. The laser source at the wavelength of 783 nm (Ondax U.S.A, model LM-783-PLR-75−1, 75 mW) is transverse magnetic (TM) polarized by a linear polarizer, so that the incident beam enters the prism with the electromagnetic fields $H_y$, $E_x$, and $E_z$.[1] The material of the prism used for the optical coupling of the SPP in the sensor chip is SF4, with a nominal value of the refractive index of 1.74 at the wavelength of 783 nm, as indicated by the manufacturer. The other side of the sensor chip is instead coupled to a flow-cell to inject the liquid forming the bulk external environment (or external medium) of the sensor with a refractive index $n_b$. More details of the experimental configuration are reported in the Supporting Information (S.1.7).

The structure of the sensor chips consists of an SF4 substrate, an adhesion layer, and a layer to support the propagation of the SPPs. All the fabricated sensor chips had a gold (Au) thin film with a nominal thickness of about 49 nm, but they have different metal−dielectric interfaces. In fact, both chromium (Cr) or MPTS were used as adhesion layer, and bare Au or Au/SLG bilayers were used to support the SPPs. The sensor chips with different metal−dielectric interfaces investigated in the present research are represented in Figure 1b−d.

In order to assess the influence of the adhesion layers and graphene layer on the performance of the SPR sensors, we considered as parameters the bulk sensitivity ($S_{RI}$) and FOM of the SPR sensors, defined as[36]

$$S_{RI} = \frac{\partial \theta_{SPR}}{\partial n_b} \text{ and } M = \frac{S_{RI}}{\text{fwhm}} \tag{1}$$

where $\theta_{SPR}$ and fwhm are the resonance angle and full width half-maximum of the reflectivity curves, respectively.

For the experimental evaluation of $S_{RI}$, the refractive index of the external medium $n_b$ was changed from 1.33 to 1.35 by mixing glycerol (gy) with deionized (DI) water in different gy:$H_2O$ volume concentrations, in a manner similar to that reported in ref 27.

## 2. THEORETICAL MODELING

**2.1. Optical Modeling of the Graphene−Gold Effective Medium ($SLG_{Au}$).** During the operation of the gold−graphene SPR sensor represented in Figure 1d, the SLG is in contact on one side with the atoms of the gold thin film and on the other side with the water molecules introduced through the flow-cell. In this case, the electronic transfer may involve both the carbon and gold atoms, and the water molecules, creating spatial charge distribution in the charge transfer region with an effective thickness $t_{eff}$, extend in both the gold thin film and water environment, as indicated in Figure 2.

Our proposal is to model such a Au/SLG/$H_2O$ interface as a homogeneous planar thin film with effective geometrical and optical properties. We call the effective homogeneous medium $SLG_{Au}$ and characterize it by a thickness $t_{eff}$ and an effective complex refractive index $N_{eff} = n_{eff} + ik_{eff}$, as commonly performed in effective medium approaches for the optical modeling of complex heterogeneous materials.[14,17]

In the Maxwell-Garnett theory, for example, the values of both $t_{eff}$ and $N_{eff}$ depend on the concept of fill factor *f*, which describes the effective volumetric inclusion of massive traces of a minor phase into a major hosting phase.[14,37] In the present case of the graphene−gold hydrated effective medium, there is not any volumetric inclusion between the different phases, but


https://doi.org/10.1021/acs.jpcc.2c02841
J. Phys. Chem. C 2022, 126, 13905−13919

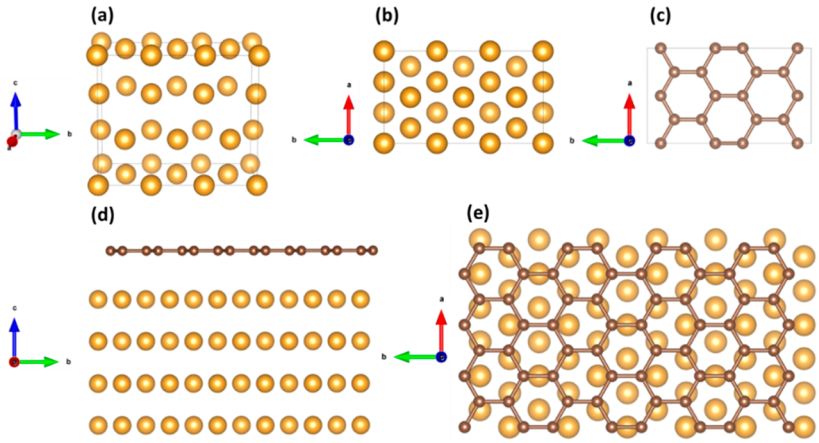


**Figure 3.** Construction of the graphene−gold (111) interface. (a) Side and (b) top views of (1 × 3 × 1) gold(111) supercell. (c) Top view of rectangular (2 × 2 × 1) supercell of graphene. (d) Side and (e) top views of optimized structure of graphene−gold (111) interface. Yellow and brown balls represent gold and carbon atoms.

there is a transfer of electrons between them, as represented in Figure 2.

It is reasonable that the graphene transfer has negligible second-order effects on the value of the dielectric constant of the substrate (gold thin film in our case), and the optical susceptivity ($\chi$) and conductivity ($\sigma$) of the SLG are instead affected by the transfer procedure and dependent on the particular choice of substrate and bulk external environment (air and water).[38−41]

The characteristic of the SPR resonance in thin metallic films is the creation of an SPP at the metal−dielectric interface, where the term polariton is attributed to the fact that the amplitude of the evanescent electric field $E_z$ along the direction perpendicular to the planar interfaces is order of magnitudes higher than the amplitude of the component $E_x$ of the electric field parallel to the plane of the thin films ($xy$ plane).[1,42] In this scenario, SPR spectroscopy is used to probe the extraordinary optical properties of the SLG along the $z$ axis, and we will denote them with the symbol ⊥.[38,43]

When electromagnetic radiation interacts with graphene, it can induce a displacement in both bound and free electrons, which we associate to $\chi^{\perp}$ and $\sigma^{\perp}$, respectively. Here, we have to remember that electron transitions for electric fields perpendicular to the plane of carbon atoms is allowed only in the ultraviolet C (UVC) region for suspended SLG (i.e., 9 eV),[43] so that the extraordinary optical conductivity of the SLG before deposition on the gold layer is zero.

In our approach, we consider the dielectric constant of the effective medium $SLG_{Au}$ after the transfer of the SLG over the gold as a perturbation of the dielectric constant of the pristine graphene. With this hypothesis we can write that[38]

$$\begin{aligned}\varepsilon_{\text{eff}}^{\perp} &= (1 + \chi_{\text{eff}}^{\perp}) + \mathrm{i}\frac{\sigma_{\text{eff}}^{\perp}}{\varepsilon_0\omega} \\ &= (1 + \chi_{\text{pristine}}^{\perp} + \Delta\chi_{\text{bound-electron}}^{\perp}) + \mathrm{i}\frac{\Delta\sigma_{\text{free-electron}}^{\perp}}{\varepsilon_0\omega}\end{aligned} \tag{2}$$

where $\chi_{\text{pristine}}^{\perp} = 1.5$ is the theoretical extraordinary susceptibility of the pristine graphene before deposition on gold[43] and $\Delta\chi_{\text{bound-electron}}^{\perp}$ and $\Delta\sigma_{\text{free-electron}}^{\perp}$ are the changes in the extraordinary susceptibility and optical conductivity after the transfer, respectively. We use the last parameters to describe from the optical point of view the effects of the charge transfer across the Au/SLG/$H_2O$ interfaces, which may induce changes in both the real part of the polarizability (bound-electron) or conductivity (free-electron) perpendicular to the carbon atoms plane. Figure 2 illustrates schematically the structure of the gold−graphene plasmonic sensors and the link between the electron transfer and the concept of graphene−gold effective medium $SLG_{Au}$.

**2.2. Protocol to Obtain the Optical Constant of the $SLG_{Au}$ by the Two-Medium Method.** To measure the effective extraordinary optical constants and thickness of the $SLG_{Au}$, we applied the traditional and robust two-media method.[35] First, we stabilized the gold thin film by immersion in water for 24 h (the reason will be clear later in the text), and subsequently we measured the experimental SPR spectra of the bare metal thin film. The latter was analyzed by the Winspall 3.02 software available online,[44] used to retrieve the values of refractive index ($n$, $k$) and thickness of the metal layer. Afterward, the SLG was transferred on the gold thin film, and two more SPR spectra were measured in the region of the samples containing the Au/SLG bilayers. These measurements were performed at two different external medium refractive indexes ($n_b$): DI water and glycerol solution in DI water.

For the determination of $N_{\text{eff}} = n_{\text{eff}} + ik_{\text{eff}}$ and $t_{\text{eff}}$ by the use of the two-medium method, we developed a code using MatLab 9.0 software based on the classical transfer matrix method.[45]

The input data of the code are the experimental values of the optical constant and thickness of the metal thin films, and the experimental angle of resonance $\theta_{\text{SPR}}$ of the Au/SLG bilayers at the different external refractive index $n_1 = 1.33$ and $n_2 = 1.35$. The code gives as output data two sets of solutions $(t_{\text{eff}}, n_{\text{eff}})_{n_1}$ and $(t_{\text{eff}}, n_{\text{eff}})_{n_2}$ for the real part of the extraordinary refractive index ($n_{\text{eff}}$) and the effective thickness ($t_{\text{eff}}$) of the $SLG_{Au}$, each one associated with the external refractive index $n_1$ and $n_2$, respectively. As reported in detail by our group for the two-thickness, two-modes, or two-color method,[14,16,46] also in the two-media method[35] the intersection point of the two curves in the $n_{\text{eff}}$ versus $t_{\text{eff}}$ plane represents the real value of the effective parameters. After that, the value of the imaginary part of $N_{\text{eff}}$, which has a second-order effect in the position of $\theta_{\text{SPR}}$, is determined by the matching of the fwhm of the experimental and theoretical SPR curves. This procedure generates an array


https://doi.org/10.1021/acs.jpcc.2c02841
J. Phys. Chem. C 2022, 126, 13905−13919

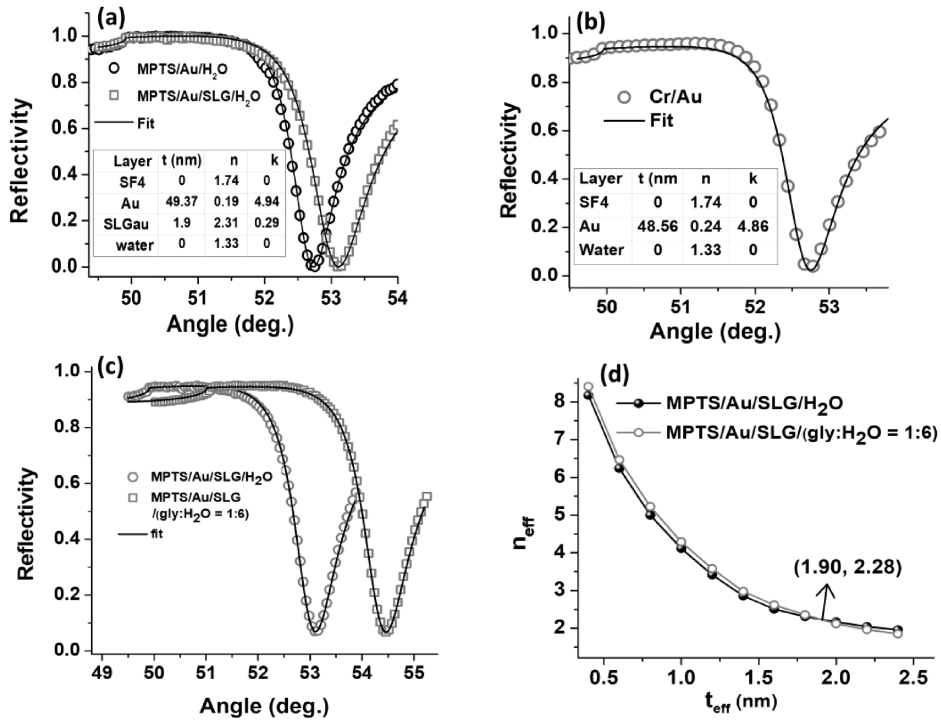


**Figure 4.** (a) SPR curve of the MPTS/Au/SLG devices before and after the SLG transfer. (b) Reflectivity spectra of the Cr/Au sample. The insets show the values of the thickness and optical constants of the different layers of the samples obtained from the theoretical fit. (c) Reflectivity spectra of the MPTS/Au/SLG samples in DI water ($H_2O$) and in glycerol solution in DI water (gy:$H_2O$ = 1:6). (d) The crossing point of the set of solutions $(t_{\mathrm{eff}}, n_{\mathrm{eff}})_{n_1}$ and $(t_{\mathrm{eff}}, n_{\mathrm{eff}})_{n_2}$ by application of the two-media method. Both the experimental and theoretical SPR curves were normalized between 0 and 1.

of vector solutions $\mathbf{s} = (t_{\mathrm{eff}}, n_{\mathrm{eff}}, k_{\mathrm{eff}})$. To calculate the experimental error, because the values of the solution vector $\mathbf{s}$ depend on the thickness and refractive index of the gold thin film, the procedure described above was repeated considering different values of the real part of the dielectric constant of the metal substrate, within the experimental accuracy in its evaluation reported in our previous works.[14,46]

The same code in MatLab 9.0 software was also used to calculate the electric field intensity distribution $|E|^2$ of the component parallel to the interfaces of the devices and to calculate the normalized shift in the SPP wavevector ($\delta k_{\mathrm{norm}}$) due to a variation of the dielectric constant of the external environment ($\delta\varepsilon_{\mathrm{ext}}$), defined with the first-order perturbation theory as[47,48]

$$\delta k_{\mathrm{norm}} = \frac{\delta k_{\mathrm{SPP}}/k_0}{\delta\varepsilon_{\mathrm{ext}}} \approx \frac{k^{\mathrm{i}}_{\mathrm{SPP}}}{2k_0\varepsilon^{\mathrm{i}}_{\mathrm{ext}}} \frac{\iiint_{V_{\mathrm{w}}} (\mathbf{E}^{\mathrm{i}*}_{\perp}\cdot\mathbf{E}^{\mathrm{f}}_{\perp})\mathrm{d}V}{\iiint_{V_{\mathrm{w}}} (\mathbf{E}^{\mathrm{i}*}_{\perp}\cdot\mathbf{E}^{\mathrm{i}}_{\perp})\mathrm{d}V} \tag{3}$$

where $V_{\mathrm{w}}$ is the volume of the water environment, $k_0 = \omega\sqrt{\mu_0\varepsilon_0}$; $k^{\mathrm{i}}_{\mathrm{SPP}}$ and $\varepsilon^{\mathrm{i}}_{\mathrm{ext}}$ are the SPP wavevector and the dielectric constant of the external environment before the change $\delta\varepsilon_{\mathrm{ext}}$; and $E^{\mathrm{i}}_{\perp}$ and $E^{\mathrm{f}}_{\perp}$ are the electric field component of the SPP perpendicular to the interface ($z$-direction) before and after the dielectric constant change, respectively.

**2.3. DFT Calculations.** The density functional theory (DFT) calculations were performed with the SIESTA code[49] using the vdW-BH functional.[50] Norm-conserving Troullier–Martins pseudopotentials for C, Au, H, and O were constructed using the ATOM code.[51] For the calculations, a vacuum layer of 25 Å has been added above the surface (graphene layer) along the slab-normal direction in order to minimize the interaction between the slab and its periodic replica. To mimic the gold–graphene interface, we considered the case when graphene was transferred to a gold (111) surface. It was revealed that the (1 × 3 × 1) gold (111) supercell matches well with rectangular (2 × 2 × 1) supercell of graphene (Figure 3a–c). Eventually, the model of the Au–graphene encompasses a single graphene layer containing 64 carbon atoms, which is placed onto the Au(111) slab containing 96 gold atoms (Figures 3d,e). It is worth noting that the bulk gold layer was simulated by considering four atomic layers of gold.

To consider the aqueous environment effect on the electronic properties of the graphene interfacing with gold as well as interfacial charge transfer, we performed additional calculations via placing water molecules above the graphene layer and in the region between graphene and gold surface. This case can be, to some extent, referred to as water intercalation beneath graphene. We employed double-ζ polarized (DZP) basis set with an energy shift of 200 meV to perform geometric optimization.As was shown in previous work,[52−55] the DZP basis set is good enough to provide reasonable results for graphene-based systems, including metal–graphene interface. Force tolerance was set to 0.02 eV/Å. A $k$-grid of 9 × 9 × 1 Monkhorst–Pack was used to sample the Brillouin zone during the optimization process. While 24 × 24 × 1 Monkhorst–Pack of $k$ points were used to perform band structure calculations.

## 3. RESULTS

**3.1. SPR Spectroscopy on $SLG_{Au}$.** The quality of the graphene grown on Cu foil by chemical vapor deposition (CVD) before and after transfer on the gold thin film was first


https://doi.org/10.1021/acs.jpcc.2c02841
J. Phys. Chem. C 2022, 126, 13905−13919

examined by Raman spectroscopy. It is worth noting that the polyurethane used for the transfer of the SLG over gold was not detected, and the results, reported in the Supporting Information (S.2.1), confirm the presence of high-quality SLG. Moreover, different from the case of copper or silver thin films,[4] the tetrahydrofuran used to remove the polyurethane does not react with the gold thin film, hence preserving the quality of the metal deposition.

After transfer of the graphene layer, we characterized the excitation of the SPPs at the Au/SLG interface. Figure 4a,b displays the SPR experimental spectrum in water of the MPTS/Au sample before and after the graphene transfer and of the Cr/Au sample without the SLG, respectively. We remember here that the SPR spectra of the samples with the organic MPTS adhesive layer of Figure 4a were measured only after the stabilization of the gold thin film in water for 24 h. The values of refractive index ($n$, $k$) and thickness of each layer used to make a theoretical fit over the experimental points are summarized in the inset tables of Figure 4a,b. In Figure 4c are represented the SPR reflectivity curves used for the implementation of the two-medium method, where the external refractive index was switched from 1.33 (DI water) to 1.35 (gy:$H_2O$ = 1:6). The crossing point of the set of solutions $(t_{eff}, n_{eff})_{n_1}$ and $(t_{eff}, n_{eff})_{n_2}$ is represented in Figure 4d. Calculating the accuracy as explained in section 3.2, we found that the effective thickness and extraordinary optical constant of the $SLG_{Au}$ effective medium are expressed by the vector solution $\mathbf{s}_{exp} = (t_{eff}, n_{eff}, k_{eff}) = (1.9 \pm 0.2$ nm, $2.3 \pm 0.2$, $0.3 \pm 0.1)$. Similar results, within the reported experimental error, were obtained for the other two samples with $SLG_{Au}$.

Table 1 reports the experimental values of the complex dielectric constant of the gold thin films in the MPTS/Au and Cr/Au interfaces, measured at $\lambda$ = 783 nm. The value relative to the Cr/Au interface is derived from the fit on the SPR experimental curve of Figure 4b, where the multilayer structure is modeled without the Cr ultrathin film of 2 nm. Its optical effect, consisting principally in the broadening of the curve and SPP damping, is reflected in the high value of the extinction coefficient of the gold, obtained by the fit of the experimental curve. In the table, $\delta\varepsilon_{i\%}$ is also reported, which represents the percentage deviation from the value of the Johnson and Christy datasheet for gold, which is considered a theoretical reference value.

**Table 1. Experimental Values of the Complex Refractive Index of the Gold Thin Films in the MPTS/Au and Cr/Au Interfaces, Measured at $\lambda$ = 783 nm**[a]

| interface | $n$ | $k$ | $\delta\varepsilon_{i\%}$ |
|---|---|---|---|
| MPTS/Au | 0.19 | 4.94 | +33 |
| Cr/Au | 0.24 | 4.86 | +65 |

[a] $\delta\varepsilon_{i\%}$ represents the percentage deviation of the imaginary part of the experimental dielectric constant from the value of the Johnson and Christy datasheet[56] for gold, considered as the theoretical reference value.

**3.2. Stability of the Interfaces of the SPR Sensors in Water.** In a previous study, we demonstrated that the stability of metal−organic interfaces in SPR sensors operating in an air environment can be enhanced by the transfer of CVD-grown graphene over the thin metal film, linked to the glass substrates by MPTS.[15,31]

In the present work, the aging effects on the metal−dielectric interfaces of the SPR sensors in DI water environment were studied for different device configurations, using metal and/or organic adhesion layers, with exposed bare metal surfaces and with graphene protection. In particular, we monitored over 24 h the shift in the SPR angle ($\Delta\theta_{SPR}$) and the change in the full width at half-maximum of the SPR reflectivity curves ($\Delta$fwhm) in different sensor configurations: (i) without adhesion and protection layer, (ii) with Cr or MPTS as an adhesion layer, and (iii) with graphene protecting layer. The measurements were repeated on a set of four samples, and the results were averaged. The results are shown in Figure 5a,b.

We highlight here that, in this case, the MPTS/Au thin film was not stabilized by immersion in pure deionized water before the SLG transfer procedure.

AFM characterization was performed to examine the morphology of the MPTS/Au interfaces after the aging process in water. We investigated the samples in several different regions corresponding to the central part of the metal thin films, where the SPPs are excited during SPR spectroscopy. Figure 6 displays the morphology (A and C) and phase (B and D) images of the surface of a 49 nm thick Au film, before and after a 44 h immersion in DI water. The fresh gold thin film deposited over the self-assembled monolayer of MPTS shows a root-mean-square (RMS) surface roughness of 1.94 nm, while the same sample after deionized water treatment over 44 h indicates a surface roughness of 1.38 nm. The AFM phase

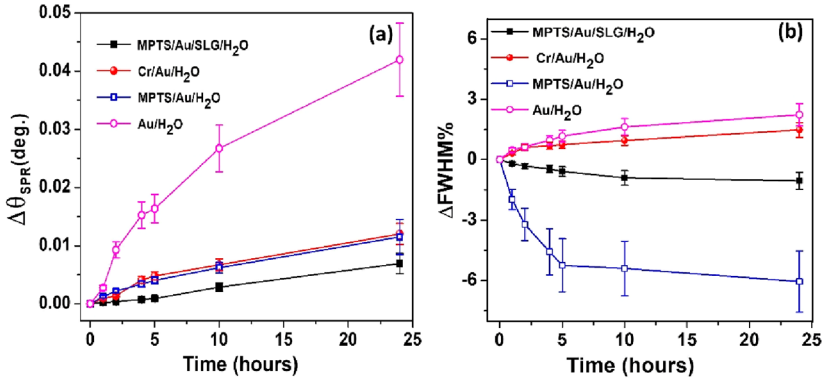


**Figure 5.** Monitoring of the shift in the SPR angle $\Delta\theta_{SPR}$ (a) and change in the full width half-maximum $\Delta$fwhm (b) relative to different interface configurations: without both adhesion layer and SLG, with Cr or MPTS as adhesion layer, and with SLG as protecting layer. The measurements were repeated on a set of four samples, and the results were averaged.


https://doi.org/10.1021/acs.jpcc.2c02841
J. Phys. Chem. C 2022, 126, 13905−13919

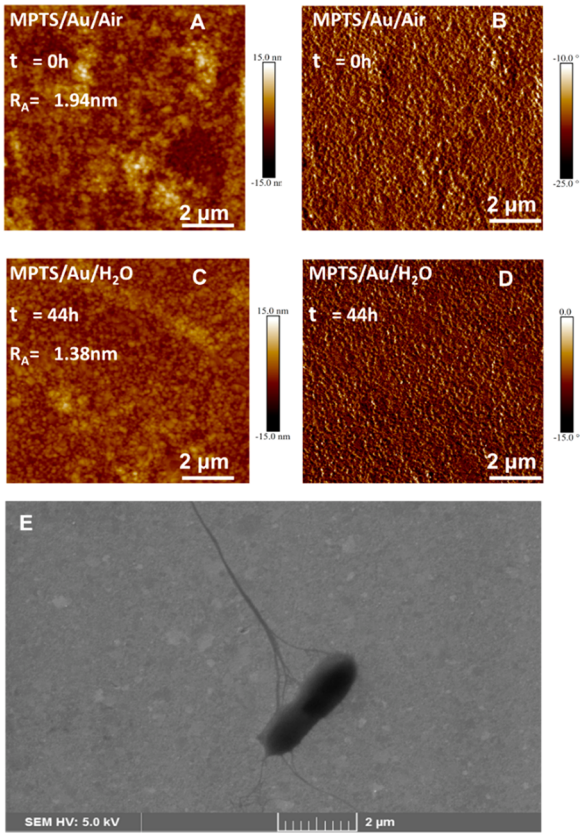


**Figure 6.** AFM images of a 49 nm thick gold film deposited over $SF_4$ glasses with MPTS as adhesion layer. Morphology (left side) and phase (right side) images were taken before (A and B) and after (C and D) immersion in DI water for 44 h. The images were taken on a surface with an extension of 10 $\mu$m × 10 $\mu$m. (E) SEM image of the typical cracks of the gold thin film after aging in water.

images before and after immersion in deionized water are uniform and did not reveal any variation that can be associated with possible chemical reactions. The results can be reproduced well over different samples.

The MPTS/Au interfaces were also studied by scanning electron microscopy (SEM), before and after aging in DI water. The samples were aged in water for 72 h in order to observe defects on the metal surface, which are not observable on the pristine samples. A typical image of the cracks in the gold thin films formed after water diffusion is reported in Figure 6E. The smaller cracks were observed in the form of irregular channels, with a thickness ranging between 50 and 200 nm. These smaller crack channels converge into bigger micrometer-sized cracks, with average size between 2 and 4 $\mu$m.

The size of the SLG domains was studied by semicontact mode AFM, performed on graphene samples on Cu foils after the growth. Panels a and b of Figure 7 show the height and the phase images, respectively. The most evident features are the metal oxide prominences perpendicular to the lamination direction of the Cu substrate and the graphene grain boundaries, clearly indicated in the panel a. Similar to the results reported in refs 57 and 58, the average linear size of the monocrystalline grains is about 7 $\mu$m, which is at least 1 order of magnitude smaller than the Cu foil grain boundaries themselves and 2 orders of magnitude smaller than the laser beam diameter using SPR spectroscopy.

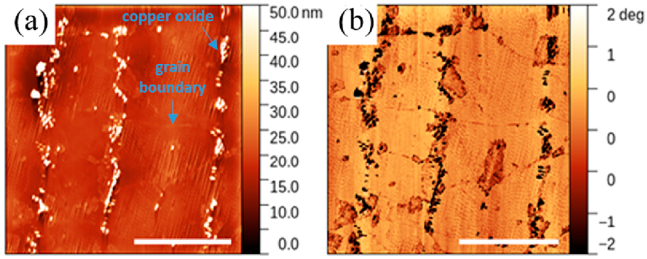


**Figure 7.** (a) Height micrograph of graphene flakes on Cu substrate as measured by AFM. The flakes are uniformly distributed over the foil and are at least 1 order of magnitude smaller than the Cu grain boundaries. (b) Phase micrographs of graphene flakes on Cu substrate as measured by AFM. The graphene flakes grain boundaries are better visualized in phase imaging (mind the darker horizontal lines). On average, the graphene flakes principal axis is 7 $\mu$m across. The scale bar in the figures corresponds to 10 $\mu$m.

**3.3. $S_{RI}$ and FOM of the Devices with Different Interface Configurations in Water.** In Figure 8a−d are shown the experimental reflectivity spectra, the experimental $S_{RI}$ and FOM, the square of the theoretical electric near field ($E^{\perp}$), and the normalized shift $\delta k_{norm}$ (eq 3) in the SPP wavevector, corresponding to the SPR sensors in the different interface configurations: aged (24 h) MPTS/Au, aged Cr/Au, and aged MPTS/Au/SLG. In the latter case, the SLG was transferred over the gold layer only after the aging process. The shift in the SPR angle $\Delta\theta_{SPR}$ of the Cr/Au, MPTS/Au/SLG, and $SLG_{Au}$ devices upon the flux of glycerol water solution at different concentrations is reported in panels a, b, and c of Figure S2, respectively.

**3.4. Charge Density Difference (CDD) at the Au/$H_2O$/SLG/$H_2O$ Interfaces.** To investigate the role of $H_2O$ molecules in the interfacial charge transfer and properties of the graphene−gold effective medium, we calculated the charge density difference (CDD) in the gold−graphene combined system by considering four possible interfacial configurations: (i) without water molecules at the heterointerface (Figure 9a); (ii) with two water molecules over the SLG (Figure 9b); (iii) two water molecules between the first atomic gold layer and the SLG (Figure 9c); (iv) two water molecules between the first atomic gold layer and the SLG and four water molecules adsorbed over the SLG, creating a Au/$H_2O$/SLG/$H_2O$ interface (Figure 9d).

## 4. DISCUSSION

**4.1. Mechanism Leading to the Interfacial Chemical Reaction with Water.** As reported in Table 1, the experimental value of the imaginary part of the dielectric constant of the gold thin film in the MPTS/Au devices matches within ∼10% with the Johnson and Christy reference data. The matching is coherent with the existence of a low-damping metal−organic interface and implies that only the de-excitation of the electron−hole pairs at the Fermi level and the prism coupling are responsible for the damping of the SPP[42] without significant additional radiative losses associated with interface defects.

Several reports advise that SPR sensors should be kept around 24 h in water to obtain it stabilization prior to use,[31] but none of these works investigated the physical−chemical processes occurring at the metal−dielectric interfaces along this transient period. As reported in Figure 5, both the resonance angle and the fwhm of the plasmonic devices change


https://doi.org/10.1021/acs.jpcc.2c02841
J. Phys. Chem. C 2022, 126, 13905−13919

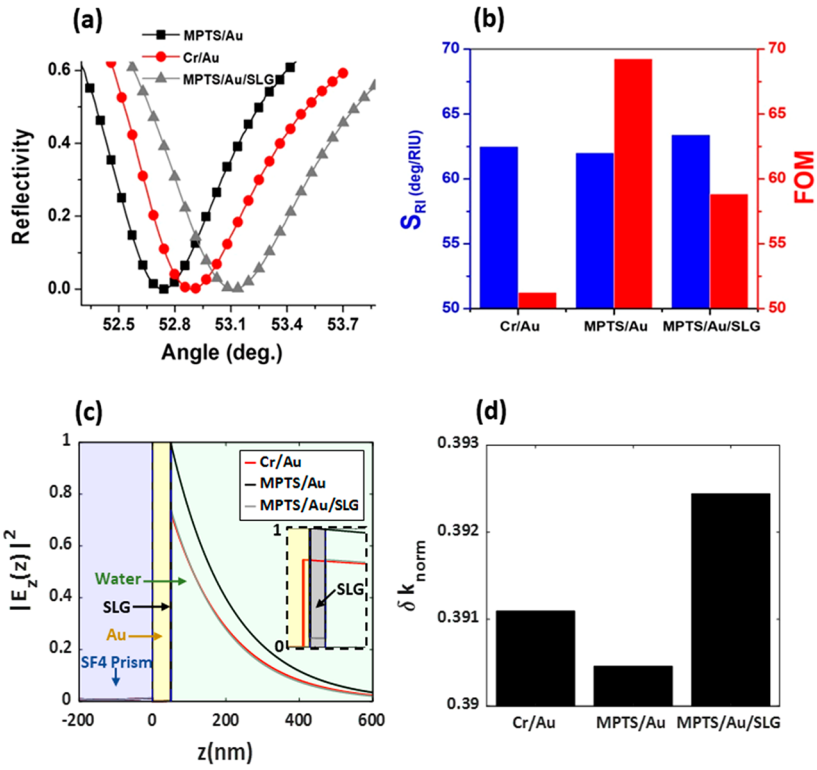


**Figure 8.** Comparison of different properties of the SPR sensors depending on the interface configurations: aged (24 h) MPTS/Au, Cr/Au, and MPTS/Au/SLG. (a) SPR reflectivity spectra normalized between 0 and 1. (b) Bulk $S_{RI}$ (blue) and FOM (red). (c) Square of the theoretical electric near field ($E^{\perp}$). (d) Normalized shift $\delta k_{norm}$ (eq 3) in the SPP wavevector. The data are relative to a wavelength of 783 nm. The values of the parameters of the devices are reported in Table 1.

during immersion in water for 24 h. The presence of metal−glass adhesion layers effectively mitigates these angular drifts. The rate of change of $\Delta\theta_{SPR}$ and Δfwhm is independent of the choice of a metal (Cr) or organic (MPTS) adhesion layer, with the exclusion of the fwhm of the MPTS/Au interfaces, for which we observe a peculiar continuous decrease of the fwhm over time.

We attribute the behavior of Figure 5 to the diffusion of water molecules through the metal thin films.[18−20] When water molecules diffuse through the channels created by the cracks in the thin films, the local optical density can be affected in different forms: (i) altering the real part of the dielectric constant of the thin films, with an overall positive shift of the angle of resonance as may be inferred by effective medium theories;[17,37] (ii) the water molecules enhance the stress of the thin film at the glass/adhesion layer/metal interface, leading to progressive delamination and formation of a water thin film at the interface, with an overall positive shift of the angle of resonance, and progressive broadening of the SPR curve; (iii) triggering chemical reactions at the glass/adhesion layer/metal interface, with eventual changes in the morphology of the thin film, and effects on the SPR reflectivity curve which should be investigated case by case.

Our observations suggest the rupture of the strained siloxane (Si−O−Si) chains of the SAM of MPTS when water molecules reach the organic adhesion layer. In fact, the electronegative oxygen of water may react with the electrophilic Si breaking the siloxane bridges, forming a silanol group (Si−OH) with a potential rearrangement of the SF4/MPTS/metal interface.[59,60] The reorganization of the metal nanostructure due to the hydration of MPTS leads to a decrease of the RMS of the metal surface of about 30%, as reported in Figure 6A,C, which is consistent with the 10% decrease in the fwhm of the SPR device after aging (Figure 5b).[42]

As was expected, the interfacial chemical reaction is highly limited after graphene transfer over the gold surface, confirming the outstanding impermeability property of graphene to gases and liquids.[4,61] Anyway, we can still observe an overall decreasing of the fwhm over 24 h of about 1%, which is reproducible on different samples and does not happen when the devices are aged in air.[31] The fwhm of the SPR curve is used in this case as the sensing parameter, indicating that water molecules are still causing chemical reactions at the SF4/MPTS/Au interface.

These observations support the scenario where water molecules may pass through the CVD grown SLG during the SPR experiments, most probably along the structural defects associated with the policrystallinity of CVD-grown SLG, as shown in Figure 7.[57] Water molecules can continue diffusing in the cracks of the metal thin film until they reach the SF4/MPTS interface and trigger the chemical reactions. The proposed mechanism is represented in Figure 10, where a stable film of a few water molecules may be formed between the SLG and Au thin film at the grain borders, similar to that demonstrated experimentally for the intercalation of water molecules between two planes of SLGs in a humid environment.[34]

**4.2. Optical Constants and Thickness of the $SLG_{Au}$ Effective Medium.** Although the SLG/substrate interaction is particularly interesting in metal substrates,[28,40] also insulators, including glass and alumina, may theoretically induce changes in the graphene electronic properties,


https://doi.org/10.1021/acs.jpcc.2c02841
J. Phys. Chem. C 2022, 126, 13905−13919

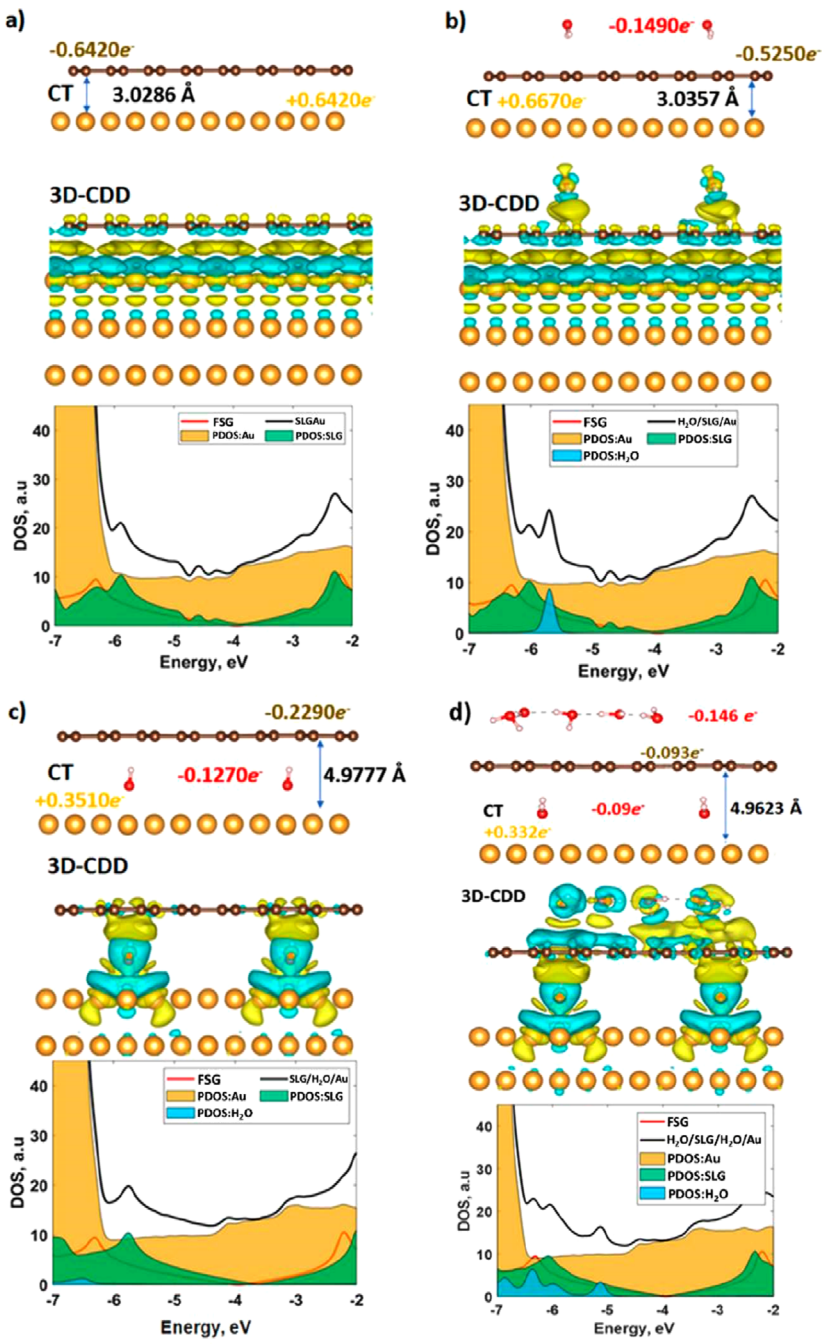


**Figure 9.** Theoretical total charge transfer (CT) predicted by VCPA and tridimensional charge density difference (3D-CDD) characterizing the Au/$H_2O$/SLG/$H_2O$ interfaces, together with the corresponding density of states (DOS) of the gold−graphene system. For comparison, DOS of free-standing graphene is also demonstrated. Yellow, brown, red, and whitish balls represent gold, carbon, oxygen, and hydrogen atoms, respectively. (a) No water molecules. (b) Two water molecules in the external environment. (c) Two water molecules in the external environment and two water molecules intercalated into the Au/SLG bilayer. (d) Bulk water as external environment and two water molecules intercalated into the Au/SLG bilayer. In all the cases, the bulk gold thin film has been simulated by four atomic gold layers, while the water external environment by the application of four layers of water molecules. In the case of the 3D-CDD, we represented the isosurfaces corresponding to 0.0005, while yellow and cyan colors correspond to positive and negative $\Delta\rho$. For the sake of simplicity, for results summarizing VCPA only one atomic layer of gold is shown in the schematic drawings. Although, as explained in the section 3.3, four atomic layers were considered in all the DFT simulations to simulate the bulk gold.

eventually leading to SLG doping.[39,40,62] This means that the thickness and optical constants of the SLG measured by SPR spectroscopy may depend on the nature of the particular substrate on which the 2D material is deposited and should always be considered in principle as effective parameters, and they are indicated as $t_{eff}$ and $N_{eff}$.

The features of the Raman spectra of the SLG over the low-damping MPTS/Au device reported in Figure S1 are coherent with the presence of high-quality monolayer graphene.[58] In this case, using the data processing reported in section 3.2, we obtain $N_{eff} = (n_{eff} + ik_{eff}) = (2.3 + i0.3)$ as the average value of the extraordinary complex refractive index of the $SLG_{Au}$. The


https://doi.org/10.1021/acs.jpcc.2c02841
J. Phys. Chem. C 2022, 126, 13905−13919

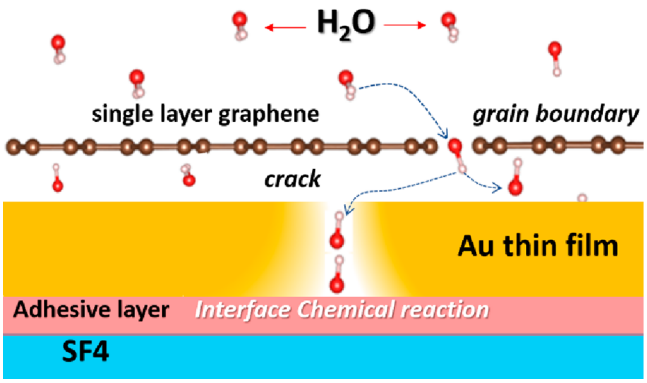


**Figure 10.** Scheme of the possible water diffusion paths at the graphene–gold heterointerface. Water molecules may have access to the adhesive layer through the grain boundaries of polycrystalline CVD graphene and the cracks present in the metal thin film. Once the adhesive interface is reached, mechanical stress and/or chemical reaction may be triggered.

results fit coherently in the large scattering of the experimental data of the refractive index of the SLG existing in the literature using different experimental techniques, as reported in Table 2. The large spread of the experimental data in the literature is in part due to a lack of differentiation of the different experimental techniques (SLG synthesis and transfer, SPR method), different external environments (air and liquid), and different substrates for the SLG analysis.[32,33,63,64]

We exclude from the discussion the experimental results obtained using spectroscopic ellipsometry in the literature because the specificity between the extraordinary and ordinary properties of the SLG is lost in this case[63,64] and the theoretical value of reference the scientific community should take into account is not clear.

In the case of SPR spectroscopy,[32,33] the theoretical reference value of the extraordinary dielectric constant of the pristine free-standing graphene is $\varepsilon^{\perp}_{\text{pristine}} = 2.5$, purely real, and independent of the wavelength in the visible and near-IR regions.[43] Cheon et al.[32] proposed the multiple measurements of reflectivity in both *s* and *p* polarization, but they assumed that the optical constants of SLG are independent of the polarization and forced a value of the effective thickness equal to the theoretical distance of two carbon layers of 0.33 nm. To measure accurately both the effective dielectric constants and thickness of thin films, the two-thickness, two-modes, or two-color SPR spectroscopy methods[14,16,46] are generally well-suited. Using a two-media method, we measured an average value of the effective thickness of the $SLG_{Au}$ in water $t_{eff} = (1.9 \pm 0.2)$ nm, which is higher than previously reported by Jussila et al. by application of a mixed two-thickness and two-color method (i.e., 1.1 nm).[33] In the latter work, the authors noticed that there is no correlation between the RMS roughness of the substrate and the value of $t_{eff}$, at least when the roughness of the substrate is in the range of the values we measured for the aged gold thin film used for the transfer of the SLG in the present work ($RMS_{Au}$ = 1.38 nm).

Reasonably, at least two important factors are controlling the experimental optical constants and $t_{eff}$ of graphene: (i) the physical interaction between SLG and substrate[28,38,39] and (ii) the eventual presence of liquid molecules in the external environment and between the SLG and the substrate.

In the special case of gold, a change in its work function of about 0.2 eV has been measured by Kelvin probe force microscopy (KPFM) in air,[27] and theoretical calculations predict that the p-doping of the SLG is associated with the hybridization of the 5d orbitals of the gold atoms and $p_z$ orbitals of SLG.[28] An enhancement in the sensitivity of the gold–graphene SPR sensors in water has been observed experimentally[27,62] and attributed to the alteration in the optical properties of the gold layer, in particular the enhancement of its plasma frequency after the electron transfer.[27] Anyway, in all the works present in the literature, the effect of the eventual presence of water molecules in the graphene-protected devices is not taken into consideration from a theoretical or experimental point of view. Moreover, because the electron transfer is an interfacial effect as pointed out by Chung et al.,[27] it is more reasonable that the bulk dielectric constant of the gold thin film is not significantly affected by the SLG transfer.

Vice versa, the DFT results reported in Figure 9 highlight that the electronic structure of the SLG may be altered by the electron transfer at the $Au/H_2O/SLG/H_2O$ interfaces in a water environment and control indeed the effective thickness $t_{eff}$ of the hybrid graphene–gold effective medium, the $SLG_{Au}$. Such a thickness undoubtedly varies if we consider the possibility that water molecules can intercalate between the SLG and the first atomic layer of gold, similar to the case of graphene bilayers in a humid environment.[34]

Considering Figure 9a, when no water molecules are present at the heterointerface, the graphene is *n*-doped, which is evidenced by Voronoi charge population analysis (VCPA), charge density difference (CDD) analysis, and density of state (DOS)/band structure calculations (Figure S3a). More specifically, we notice the significant upshift of the Fermi level of graphene with respect to the position of the Dirac point. It is worth noting that the SLG/Au(111) interface can exhibit both *p*- and *n*-type character, by small variation of the gold–graphene distance (turning point around 0.32 nm).[28,65]

**Table 2. Example of Values of $t_{eff}$, $n_{eff}$, and $k_{eff}$ Reported in the Literature, Depending on Different Experimental Techniques, Substrates, and External Environment**

| characterization technique | graphene synthesis | substrate | environment | $t_{eff}$ (nm) | $n_{eff}$ | $k_{eff}$ |
|---|---|---|---|---|---|---|
| SPR (this work) 783 nm | CVD | Au(50 nm) | DI water | 1.9 ± 0.2 | 2.3 ± 0.2 | 0.3 ± 0.1 |
| SPR[32] | CVD | Au(50 nm)/$SiO_2$ | air | 0.33 (default) | 2.7 | 1.3 |
| 634 nm | | | | | | |
| SPR[33] | CVD | | | | | |
| 670 nm | | Au(50 nm) | air | 1.1 (first SLG) | 3.1 | 0.5 |
| 785 nm | | Au(50 nm)/$Al_2O_3$ | air | 0.8 (first SLG) | 3.1 | 0.9 |
| ellispometry[63] | exfoliated | $SiO_2$ | air | 0.34 nm (default) | 3.0 | proportional to $\lambda/n$ |
| ellipsometry[64] | exfoliated | $SiO_2$ | air | 0.34 nm (default) | 2.8 (780 nm) | proportional to $\lambda/n$ |


https://doi.org/10.1021/acs.jpcc.2c02841
J. Phys. Chem. C 2022, 126, 13905−13919

Once two water molecules were adsorbed above the graphene layer (Figure 9b), significant charge redistribution takes place at the metal−carbon interface followed by slight increase in the gold−graphene distance. According to charge population analysis, water molecules behave themselves as *p*-type dopants with respect to the graphene layer (according to VCPA, they accept $-0.15e^-$ from the underlying carbon network). The molecular orbital of the $H_2O$ is seen as a sharp peak below the Fermi level in the DOS of the Au/SLG/$H_2O$ system. It is, however, important to emphasize that the water molecule position with respect to the graphene layer may affect the charge transfer direction, as was demonstrated for free-standing graphene.[65−67] Back to our case, irrespectively to partial transfer of electrons from graphene to water molecules, the graphene is still *n*-doped because of a dominating role of electron donation from the gold substrate (Figure S3b).

Intercalation of water molecules beneath the graphene layer (Figure 9c) resulted in weakening of the graphene−gold interaction, which was manifested as a significant increase in gold−graphene distance (up to ∼5 Å), reduction of the total charge transferred from gold to graphene, decrease in energy difference between Fermi level and Dirac point position (Figure S3c), and disappearance of DOS features within the energy range from −5 to −4 eV.

When the graphene is surrounded with water molecules from both sides (Figure 9d), because of water-induced charge redistribution at the interface, the graphene becomes less negatively charged, which is additionally evidenced by further decrease in the energy difference between the Fermi level and the Dirac point position (Figure S3d). Although the presence of water molecules above graphene does not significantly affect the graphene−gold distance in comparison to the case of Figure 9c, it definitively influences the extension of the CDD. The latter extends in Figure 9d from the top of the water molecules to the second atomic layer of gold, in a spatial region with a thickness of about 1.1 nm, which represents the theoretical value of the effective thickness $t_{eff}$ of the graphene−gold effective medium.

The effect of the n- or p-type doping on the extraordinary optical response of the $SLG_{Au}$ is not clear, and no theoretical predictions can be found in the literature. The electron transfer, while cannot alter significantly the dielectric constant of gold, is expected to have a considerable effect on the optical properties of the 2D material. In the case of n-doping, such as that inferred from the DFT results, two main behaviors are expected from the transferred electrons: they may participate in the plasma transversal oscillations perpendicular to the carbon atoms plane, offering an effective extraordinary optical conductivity of the $SLG_{Au}$, or vice versa, acting like the electrons of free-standing graphene, which have a bonding character along the extraordinary axis.

From the experimental results of $N_{eff}$ at the wavelength of 783 nm, we obtain $\varepsilon_{eff}^{\perp} = (4.95 + 1.51I)$ and $\Delta\chi_{bound\text{-}electron}^{\perp} = 2.45$. The extraordinary optical susceptibility (polarizability) in water environment is highly increased, indicating a prominent electron-bound behavior of the transferred electrons. In contrast, the extraordinary optical conductivity of the SLG is almost an order of magnitude lower than the well-known ordinary universal optical conductivity.[68] The origin of this residual extraordinary optical conductivity is unclear, and we cannot exclude possible interfacial defects during the deposition of the SLG over the low-damping MPTS/Au thin film, which may be responsible for a scattering contribution of the imaginary part of the dielectric constant.[42]

Looking at Table 2, it is interesting to note that the work of Jussila et al.[33] and the present research represent the only reports in the literature where the thickness of the $SLG_{Au}$ is not considered with the default value of ∼0.33 nm, because in both cases a proper two-configuration SPR method is applied for the simultaneous determination of $t_{eff}$ and $n_{eff}$. Concerning our case, we think that the qualitative matching between the theoretical DFT (1.1 nm) and experimental SPR (1.9 ± 0.2 nm) values of the effective thickness $t_{eff}$ is in part due to the fact that we are simulating the external water environment by the adsorption of four water molecules over the surface of the graphene supercell. Increasing the surface density of molecules and the number of molecular layers of water over the SLG would induce in fact a larger region with a net charge density difference (CDD). The limiting case corresponds to the formation of a capacitive double layer composed of water molecules and goes beyond the scope of the present research. Nevertheless, our DFT results show that water molecules in the external environment or inside the $SLG_{Au}$ cavity are responsible for a dynamic enhancement of $t_{eff}$ and a progressive reduction of the n-doping of the SLG. Following our optical model, n-doping reduction is associated with a lower value of $n_{eff}$, which is confirmed by the comparison between the experimental results in air and water environments.

**4.3. $S_{RI}$ and FOM of the Au Thin-Film Devices with Different Interfaces.** In Table 3, we compare the $S_{RI}$, FOM, and normalized shift ($\delta k_{norm}$) in the SPP wavevector relative to the aged SF4/Cr/Au, SF4/MPTS/Au, and SF4/MPTS/Au/SLG devices.

**Table 3. $S_{RI}$, FOM, and Normalized Shift $\delta k_{norm}$ in the SPP Wavevector Associated with the Different Interface Configurations in the Near-Infrared Region ($\lambda$ = 783 nm)**

| interfaces | $S_{RI}$ (deg/RIU) | FOM ($RIU^-$) | $\delta k_{norm}$ |
|---|---|---|---|
| MPTS/Au | 62.0 | 68 | 0.390 |
| Cr/Au | 62. 5 | 51 | 0.391 |
| MPTS/Au/SLG | 63.4 | 58 | 0.393 |

It is known that the presence of the metallic Cr adhesive layer broadens and distorts the SPR curve[69] because of enhanced absorption of plasmon resonance energy at the SF4 glass interface, which is responsible for the high value of the imaginary part the dielectric constant of the Cr/Au interface reported in Table 1. The enhanced absorption is related to the intrinsic higher imaginary part of the dielectric constant of Cr and intermetallic diffusion of Cr into the Au thin film during e-beam deposition, leading to a nanostructured metal−dielectric interface, which acts like an SPP scatterer.[11] For these reasons, when Cr is used as an adhesion layer, the lowest FOM of about 51 $RIU^{-1}$ is measured.

A FOM increment of about 30% is observed for devices with MPTS/Au interface without SLG transfer (∼68 $RIU^{-1}$), which is attributed to the low-damping SPP interfaces obtained after the reorganization of the nanostructured gold film during the aging process. A smaller fwhm leads in fact to a sharper Lorentzian profile of the SPR reflectivity curve and decreased SPP damping.[7] The reduction of chemical interface damping when organic molecular layers are used is consistent, for example, with the observations reported by Shen and co-workers,[70] where a narrower LSPR line width was observed for


https://doi.org/10.1021/acs.jpcc.2c02841
J. Phys. Chem. C 2022, 126, 13905−13919

gold nanocylinders fabricated on glass using MPTS as an adhesion layer. In our case, the FOM reached by the low-damping MPTS/Au devices coincides with the maximum theoretical FOM of gold SPR sensors operating in our identical experimental configuration, because of the excellent optical quality of the metal−organic interface.[71]

Observing Figure 8b, we realize that while the bulk sensitivity of the MPTS-based devices is increased by about ∼ 2% after the SLG transfer ($S_{RI}$ = 63.4 deg RIU$^{-1}$), the FOM is instead reduced. In the few literature contributions available at the moment, the enhancement in the bulk $S_{RI}$ of the $SLG_{Au}$ is associated theoretically with the enhancement in the plasma frequency of the gold layer, because of the formation of the surface dipole distribution at the Au/SLG interface in the air,[27,28] similar to the case of special gold−carbon nanocomposites.[72,73] In the literature, the increase in the sensitivity depends on the number of graphene layers transferred over the metal thin film and the wavelength of the SPP and may be negligible at telecommunication wavelengths.[27,30,64]

The decrease in FOM associated with increased sensitivity is not new in 2D-materials supported plasmonics,[74] and in most cases the effective result after 2D material transfer is similar to the deposition of a very thin layer film (<10 nm) with high refractive index over the external surface of SPR devices, which enhances the near electric field integral expressed by eq 3.[45] To further support our proposal, we link through Figure 8c,d the sensitivity of the devices with different interface configurations to the electromagnetic near-field distribution in the external environment, which controls the value of the normalized shift in the SPP wavevector $\delta k_{norm}$,[45] reported in panel d. We observe the same trend in the histograms relative to the value of $S_{RI}$ and $\delta k_{norm}$ for the different experimental configurations, represented in panels b and d of Figure 8, respectively. This result further supports the observed increment in the real part of the extraordinary refractive index of SLG after the transfer on the gold thin film and the predominant bonding behavior of the electrons transferred at their interface.

## 5. CONCLUSIONS

We investigated the effects of water diffusion on the optical and morphological properties of gold−graphene plasmonic sensors using different metal−dielectric interfaces. For each type of interface, water diffusion provokes a transient period of about 24 h, during which both the resonance angle and the fwhm of the SPR curve change. While the chromium adhesion layer provokes severe SPP damping, the use of MPTS as organic transparent ligand leads to a progressive decrease of the fwhm of the SPR curve of about 10%. AFM measurements indicate that such a decrease is due to the redistribution of the nanostructured gold thin films in water, with the formation of a low-damping SPP interface with reduced RMS roughness and high value of FOM.

We explain this particular behavior by the diffusion into the gold thin film of water molecules that, after reaching the MPTS/Au interface, possibly triggers the hydroxylation of the siloxane group of MPTS. The interfacial chemical reaction is hence used to monitor the diffusion of water molecules after SLG transfer on MPTS/Au interfaces, indicating the water can indeed pass through the crystal-border of polycrystalline CVD grown graphene.

Different from other works in the literature, we consider that the electron transfer does not influence the plasma frequency of the bulk gold layer but instead creates an extended charge redistribution region crossing the $Au/H_2O/SLG/H_2O$ heterointerface on both sides of the graphene, defining the physical region of an ultrathin effective medium $SLG_{Au}$.

Considering the DFT results, one can conclude that the nanoscale spatial charge distribution at the gold−graphene interface is highly sensitive to the presence of water molecules and results in n-type doping of the SLG. Theoretically, this makes possible the tuning of the effective thickness of $t_{eff}$ via adjusting environmental conditions like humidity or the size of the crystal grain of the CVD-grown SLG, which should control the average density of water molecules in the $SLG_{Au}$ effective medium.

From the optical point of view, we propose a simplified effective medium approach, where the interaction between the gold thin film, water molecules, and the SLG is associated with the changes in the extraordinary optical susceptivity ($\chi^{\perp}$) and conductivity ($\sigma^{\perp}$) of the 2D material.

The effective thickness and refractive index of the $SLG_{Au}$ are hence measured by the application of the two-medium method at the wavelength of 783 nm, showing that the charge redistribution crossing the $Au/H_2O/SLG/H_2O$ heterointerface is equivalent to the formation of an ultrathin effective medium with a thickness of about 1.9 nm. In comparison to the theoretical value of the pristine SLG, the effective medium shows an increment $\Delta\chi^{\perp}_{bound\text{-}electron} \simeq 2.45$ in the extraordinary optical susceptivity, indicating that the transferred electrons have a substantial bound character for TM polarization. In this panorama, the enhancement of the sensitivity of the $SLG_{Au}$ is principally attributed to the high value of the real part of the refractive index of the effective medium and the modification of the distribution of the electromagnetic field of the SPP at the metal−dielectric interface.

The results definitively highlight the importance of giving deeper attention to the interaction of the SLG with both the substrate and water molecules in order to correctly predict the optical or electronic properties of metal−graphene interfaces.

## ■ ASSOCIATED CONTENT

### Supporting Information

The Supporting Information is available free of charge at https://pubs.acs.org/doi/10.1021/acs.jpcc.2c02841.

Materials; fabrication of SPR sensing platforms; graphene synthesis and transfer over SPR platforms; Raman spectroscopy; AFM measurements; SEM measurements; experimental scheme of SPR spectrometer; Raman spectroscopy on $SLG_{Au}$; $S_{RI}$ of the plasmonic devices with different interface configurations in water; and SLG band structure at the $Au/H_2O/SLG/H_2O$ interfaces (PDF)

## ■ AUTHOR INFORMATION


### Corresponding Author

**Tommaso Del Rosso** − *Department of Physics, Pontifícia Universidade Católica do Rio de Janeiro, 22451-900 Rio de Janeiro, Brazil;* orcid.org/0000-0002-0600-4139; Email: tommaso@puc-rio.br

### Authors

**Quaid Zaman** − *Department of Physics, Pontifícia Universidade Católica do Rio de Janeiro, 22451-900 Rio de Janeiro, Brazil; Department of Physics, University of Buner, Buner 17290, Pakistan*

**Tahir** − *Department of Physics, Pontifícia Universidade Católica do Rio de Janeiro, 22451-900 Rio de Janeiro, Brazil;* orcid.org/0000-0001-6565-5030
**Fernando Lazaro Freire, Jr.** − *Department of Physics, Pontifícia Universidade Católica do Rio de Janeiro, 22451-900 Rio de Janeiro, Brazil*
**Ivan Shtepliuk** − *Semiconductor Materials Division, Department of Physics, Chemistry and Biology-IFM, Linköping University, S-58183 Linköping, Sweden;* orcid.org/0000-0002-8685-3332
**Andre N. Barbosa** − *Department of Physics, Pontifícia Universidade Católica do Rio de Janeiro, 22451-900 Rio de Janeiro, Brazil*
**Marcelo E. H. Maia da Costa** − *Department of Physics, Pontifícia Universidade Católica do Rio de Janeiro, 22451-900 Rio de Janeiro, Brazil*
**Cesar Augusto Diaz Mendoza** − *Department of Physics, Pontifícia Universidade Católica do Rio de Janeiro, 22451-900 Rio de Janeiro, Brazil;* orcid.org/0000-0003-4391-6855
**Jefferson F. D. F Araujo** − *Department of Physics, Pontifícia Universidade Católica do Rio de Janeiro, 22451-900 Rio de Janeiro, Brazil*
**Guilherme C. Concas** − *Department of Physics, Pontifícia Universidade Católica do Rio de Janeiro, 22451-900 Rio de Janeiro, Brazil*
**Marco Cremona** − *Department of Physics, Pontifícia Universidade Católica do Rio de Janeiro, 22451-900 Rio de Janeiro, Brazil*
**Zubair Ahmed** − *Department of Physics, Pontifícia Universidade Católica do Rio de Janeiro, 22451-900 Rio de Janeiro, Brazil*
**Omar Ginoble Pandoli** − *Department of Chemistry, Pontifícia Universidade Católica do Rio de Janeiro, 22451-900 Rio de Janeiro, Brazil; Dipartimento di Farmacia, Università degli Studi di Genova, 16148 Genova, Italy;* orcid.org/0000-0002-2220-7817
**Ricardo Q. Aucelio** − *Department of Chemistry, Pontifícia Universidade Católica do Rio de Janeiro, 22451-900 Rio de Janeiro, Brazil*
**Victor Dmitriev** − *Department of Electrical Engineering, Federal University of Pará, Belém, PA 66075-110, Brazil*
**Karlo Q. da Costa** − *Department of Electrical Engineering, Federal University of Pará, Belém, PA 66075-110, Brazil*
**André Felipe S. Cruz** − *Department of Electrical Engineering, Federal University of Pará, Belém, PA 66075-110, Brazil*
**Gabriella Fibbi** − *Department of Experimental and Clinical Biomedical Sciences School of Health Sciences, University of Florence-Viale G.B. Morgagni, 50−50134 Florence, Italy*
**Anna Laurenzana** − *Department of Experimental and Clinical Biomedical Sciences School of Health Sciences, University of Florence-Viale G.B. Morgagni, 50−50134 Florence, Italy*
**Francesca Margheri** − *Department of Experimental and Clinical Biomedical Sciences School of Health Sciences, University of Florence-Viale G.B. Morgagni, 50−50134 Florence, Italy*
**Anastasia Chillà** − *Department of Experimental and Clinical Biomedical Sciences School of Health Sciences, University of Florence-Viale G.B. Morgagni, 50−50134 Florence, Italy*
**Francesca Scavone** − *Department of Experimental and Clinical Biomedical Sciences School of Health Sciences, University of Florence-Viale G.B. Morgagni, 50−50134 Florence, Italy*
**Elena Frediani** − *Department of Experimental and Clinical Biomedical Sciences School of Health Sciences, University of Florence-Viale G.B. Morgagni, 50−50134 Florence, Italy*
**Rajwali Khan** − *Department of Physics, University of Lakki Marwat, Lakki Marwat 28420 Khyber Pakhtunkhwa, Pakistan*
**Nicola Daldosso** − *Department of Informatics, Università di Verona, I-37134 Verona, Italy*
**Elena Chistè** − *Department of Informatics, Università di Verona, I-37134 Verona, Italy;* orcid.org/0000-0002-7302-253X
**Gino Mariotto** − *Department of Informatics, Università di Verona, I-37134 Verona, Italy;* orcid.org/0000-0002-0035-1404
**Evelyn C. S. Santos** − *Brazilian Center for Research in Physics (CBPF), 22290-180 Rio de Janeiro, Brazil*

Complete contact information is available at: https://pubs.acs.org/10.1021/acs.jpcc.2c02841

### Notes

The authors declare no competing financial interest.

## ■ ACKNOWLEDGMENTS

This study was financed in part by the Coordenação de Aperfeiçoamento de Pessoal de Nível Superior - Brasil (CAPES) - Finance Code 001. Funding from FAPERJ for processes E-26/010.100622/2018, E-26/010.001646/2019, E-26/010.002138/2019, E-26/010.000980/2019, E-26/202.357/2019, and E-26/211.540/2021 is acknowledged. We acknowledge also CNPq and the Instituto Nacional de Engenharia de Superfícies (INCT-INES) (Processes 423349/2018-0 and 465423/2014-0). I.S. acknowledges the support from Ångpanneföreningens Forskningsstiftelse (Grant 21-112). All DFT calculations were enabled by resources provided by the Swedish National Infrastructure for Computing (SNIC), partially funded by the Swedish Research Council through Grant Agreement No. 2018-05973. The research leading to these results has received funding from AIRC under IG 2020 - ID. 24381 project − P.I. Fibbi Gabriella. The authors thank the LABNANO/CBPF for technical support during electron microscopy work.

## ■ REFERENCES

(1) Maier, S. A. *Plasmonics: Fundamentals and Applications*; 2007.
(2) Homola, J. On the Sensitivity of Surface Plasmon Resonance Sensors with Spectral Interrogation. *Sensors Actuators B Chem.* **1997**, *41*, 207−211.
(3) Sukham, J.; Takayama, O.; Lavrinenko, A. V.; Malureanu, R. High-Quality Ultrathin Gold Layers with an APTMS Adhesion for Optimal Performance of Surface Plasmon Polariton-Based Devices. *ACS Appl. Mater. Interfaces* **2017**, *9*, 25049−25056.
(4) Kravets, V. G.; Jalil, R.; Kim, Y.-J.; Ansell, D.; Aznakayeva, D. E.; Thackray, B.; Britnell, L.; Belle, B. D.; Withers, F.; Radko, I. P.; et al. Graphene-Protected Copper and Silver Plasmonics. *Sci. Rep.* **2015**, *4*, 5517.
(5) Choi, S. H.; Kim, Y. L.; Byun, K. M. Graphene-on-Silver Substrates for Sensitive Surface Plasmon Resonance Imaging Biosensors. *Opt. Express* **2011**, *19*, 458−466.
(6) Bauch, M.; Toma, K.; Toma, M.; Zhang, Q.; Dostalek, J. Plasmon-Enhanced Fluorescence Biosensors: A Review. *Plasmonics* **2014**, *9*, 781−799.
(7) Habteyes, T. G.; Dhuey, S.; Wood, E.; Gargas, D.; Cabrini, S.; Schuck, P. J.; Alivisatos, A. P.; Leone, S. R. Metallic Adhesion Layer

Induced Plasmon Damping and Molecular Linker as a Nondamping Alternative. *ACS Nano* **2012**, *6*, 5702−5709.
(8) Todeschini, M.; Bastos da Silva Fanta, A.; Jensen, F.; Wagner, J. B.; Han, A. Influence of Ti and Cr Adhesion Layers on Ultrathin Au Films. *ACS Appl. Mater. Interfaces* **2017**, *9*, 37374−37385.
(9) Debu, D. T.; Ghosh, P. K.; French, D.; Herzog, J. B. Surface Plasmon Damping Effects Due to Ti Adhesion Layer in Individual Gold Nanodisks. *Opt. Mater. Express* **2017**, *7*, 73.
(10) Colas, F.; Barchiesi, D.; Kessentini, S.; Toury, T.; Chapelle, M. L. D. La. Comparison of Adhesion Layers of Gold on Silicate Glasses for SERS Detection. *J. Opt.* **2015**, *17*, 114010.
(11) Madsen, S. J.; Esfandyarpour, M.; Brongersma, M. L.; Sinclair, R. Observing Plasmon Damping Due to Adhesion Layers in Gold Nanostructures Using Electron Energy Loss Spectroscopy. *ACS Photonics* **2017**, *4*, 268−274.
(12) Muniz-Miranda, M.; Del Rosso, T.; Giorgetti, E.; Margheri, G.; Ghini, G.; Cicchi, S. Surface-Enhanced Fluorescence and Surface-Enhanced Raman Scattering of Push−Pull Molecules: Sulfur-Functionalized 4-Amino-7-Nitrobenzofurazan Adsorbed on Ag and Au Nanostructured Substrates. *Anal. Bioanal. Chem.* **2011**, *400*, 361−367.
(13) Špringer, T.; Ermini, M. L.; Špačková, B.; Jabloňků, J.; Homola, J. Enhancing Sensitivity of Surface Plasmon Resonance Biosensors by Functionalized Gold Nanoparticles: Size Matters. *Anal. Chem.* **2014**, *86*, 10350−10356.
(14) Zaman, Q.; Souza, J.; Pandoli, O.; Costa, K. Q.; Dmitriev, V.; Fulvio, D.; Cremona, M.; Aucelio, R. Q.; Fontes, G.; Del Rosso, T. Two-Color Surface Plasmon Resonance Nanosizer for Gold Nanoparticles. *Opt. Express* **2019**, *27*, 3200.
(15) Del Rosso, T.; Zaman, Q.; Cremona, M.; Pandoli, O.; Barreto, A. R. J. SPR Sensors for Monitoring the Degradation Processes of Eu(Dbm)3(Phen) and Alq3thin Films under Atmospheric and UVA Exposure. *Appl. Surf. Sci.* **2018**, *442*, 759−766.
(16) Zaman, Q.; S. Costa, J.; Tahir; R. J. Barreto, A.; F. D. F. Araujo, J.; D. Carlos, L.; N. Carneiro Neto, A.; Cremona, M.; Ahmed, Z.; S. Cruz, A. F.; et al. Dielectric-Loaded Waveguides as Advanced Platforms for Diagnostics and Application of Transparent Thin Films. *Langmuir* **2021**, *37*, 3248−3260.
(17) Costa, J.; Zaman, Q.; Q. da Costa, K.; Dmitriev, V.; Pandoli, O.; Fontes, G.; Del Rosso, T. Limits of the Effective Medium Theory in Particle Amplified Surface Plasmon Resonance Spectroscopy Biosensors. *Sensors* **2019**, *19*, 584.
(18) Lee, C.-C. *Moisture Adsorption and Optical Instability in Thin Film Coatings*; The University of Arizona, 1983.
(19) Lin, Y.; Vlassak, J. J.; Tsui, T. Y.; McKerrow, A. J. Environmental Effects on Subcritical Delamination of Dielectric and Metal Films from Organosilicate Glass (OSG) Thin Films. *MRS Proc.* **2002**, *766*, 941−946.
(20) Khanna, V. K. Adhesion−Delamination Phenomena at the Surfaces and Interfaces in Microelectronics and MEMS Structures and Packaged Devices. *J. Phys. D. Appl. Phys.* **2011**, *44*, No. 034004.
(21) Waters, P.; Volinsky, A. A. Stress and Moisture Effects on Thin Film Buckling Delamination. *Exp. Mech.* **2007**, *47*, 163−170.
(22) Gerberich, W. W.; Cordill, M. J. Physics of Adhesion. *Rep. Prog. Phys.* **2006**, *69*, 2157.
(23) Herrmann, W. C.; Morton, D. E. Thin-Film Optical Coating Filter Stability under Different Environmental Conditions. *Appl. Opt.* **1993**, *32*, 5673.
(24) Lee, C. H.; Kim, J.-H.; Zou, C.; Cho, I. S.; Weisse, J. M.; Nemeth, W.; Wang, Q.; van Duin, A. C. T.; Kim, T.-S.; et al. Peel-and-Stick: Mechanism Study for Efficient Fabrication of Flexible/Transparent Thin-Film Electronics. *Sci. Rep.* **2013**, *3*, 2917.
(25) Lane, M. W.; Snodgrass, J. M.; Dauskardt, R. H. Environmental Effects on Interfacial Adhesion. *Microelectron. Reliab.* **2001**, *41*, 1615−1624.
(26) Giorgetti, E.; Margheri, G.; Delrosso, T.; Sottini, S.; Muniz-Miranda, M.; Innocenti, M. A Study of the Degradation of Poly(3-Octylthiophene)-Based Light Emitting Diodes by Surface Enhanced Raman Scattering. *Appl. Phys. B: Laser Opt.* **2004**, *79*, 603−609.
(27) Chung, K.; Lee, J. S.; Kim, E.; Lee, K.-E.; Kim, K.; Lee, J.; Kim, D.; Kim, S. O.; Jeon, S.; Park, H.; et al. Enhancing the Performance of Surface Plasmon Resonance Biosensor via Modulation of Electron Density at the Graphene-Gold Interface. *Adv. Mater. Interfaces* **2018**, *5*, 1800433.
(28) Giovannetti, G.; Khomyakov, P. A.; Brocks, G.; Karpan, V. M.; van den Brink, J.; Kelly, P. J. Doping Graphene with Metal Contacts. *Phys. Rev. Lett.* **2008**, *101*, No. 026803.
(29) Salihoglu, O.; Balci, S.; Kocabas, C. Plasmon-Polaritons on Graphene-Metal Surface and Their Use in Biosensors. *Appl. Phys. Lett.* **2012**, *100*, 213110.
(30) Chen, S.; Lin, C. Sensitivity Analysis of Graphene Multilayer Based Surface Plasmon Resonance Biosensor in the Ultraviolet, Visible and Infrared Regions. *Appl. Phys. A: Mater. Sci. Process.* **2019**, *125*, 230.
(31) Del Rosso, T.; Zaman, Q.; Romani, E. C.; Pandoli, O.; Aucelio, R. Q.; Melo de Lima, L.; Cremona, M.; Dmitriev, V.; Queiroz da Costa, K.; Lazaro Freire, F.; Maia da Costa, M. E. H. Enhanced Stability of Plasmonic Metal Thin Films by CVD Grown Graphene Transfer. *Thin Solid Films* **2017**, *644*, 65−70.
(32) Cheon, S.; Kihm, K. D.; Kim, H. G.; Lim, G.; Park, J. S.; Lee, J. S. How to Reliably Determine the Complex Refractive Index (RI) of Graphene by Using Two Independent Measurement Constraints. *Sci. Rep.* **2015**, *4*, 6364.
(33) Jussila, H.; Yang, H.; Granqvist, N.; Sun, Z. Surface Plasmon Resonance for Characterization of Large-Area Atomic-Layer Graphene Film. *Optica* **2016**, *3*, 151.
(34) Qadir, A.; Sun, Y. W.; Liu, W.; Oppenheimer, P. G.; Xu, Y.; Humphreys, C. J.; Dunstan, D. J. Effect of Humidity on the Interlayer Interaction of Bilayer Graphene. *Phys. Rev. B* **2019**, *99*, No. 045402.
(35) de Bruijn, H. E.; Altenburg, B. S. F.; Kooyman, R. P. H.; Greve, J. Determination of Thickness and Dielectric Constant of Thin Transparent Dielectric Layers Using Surface Plasmon Resonance. *Opt. Commun.* **1991**, *82*, 425−432.
(36) Homola, J.; Yee, S. S.; Gauglitz, G. Surface Plasmon Resonance Sensors: Review. *Sensors Actuators, B Chem.* **1999**, *54*, 3.
(37) Niklasson, G. A.; Granqvist, C. G.; Hunderi, O. Effective Medium Models for the Optical Properties of Inhomogeneous Materials. *Appl. Opt.* **1981**, *20*, 26.
(38) Wang, F.; Shi, S. Optical Properties of Graphene. In *2D Materials: Properties and Devices*; Cambridge University, Cambridge, 2017; pp 38−51.
(39) Dahal, A.; Addou, R.; Azcatl, A.; Coy-Diaz, H.; Lu, N.; Peng, X.; de Dios, F.; Kim, J.; Kim, M. J.; Wallace, R. M.; Batzill, M. Seeding Atomic Layer Deposition of Alumina on Graphene with Yttria. *ACS Appl. Mater. Interfaces* **2015**, *7*, 2082−2087.
(40) Omiciuolo, L.; Hernández, E. R.; Miniussi, E.; Orlando, F.; Lacovig, P.; Lizzit, S.; Menteş, T. O.; Locatelli, A.; Larciprete, R.; Bianchi, M.; et al. Bottom-up Approach for the Low-Cost Synthesis of Graphene-Alumina Nanosheet Interfaces Using Bimetallic Alloys. *Nat. Commun.* **2014**, *5*, 5062.
(41) Bertoni, G.; Calmels, L.; Altibelli, A.; Serin, V. First-Principles Calculation of the Electronic Structure and EELS Spectra at the Graphene/Ni(111) Interface. *Phys. Rev. B* **2005**, *71*, No. 075402.
(42) Raether, H. *Surface Plasmons on Smooth and Rough Surfaces and on Gratings*; Springer Tracts in Modern Physics; Springer: Berlin, 1988; Vol. *111*.
(43) Klintenberg, M.; Lebègue, S.; Ortiz, C.; Sanyal, B.; Fransson, J.; Eriksson, O. Evolving Properties of Two-Dimensional Materials: From Graphene to Graphite. *J. Phys.: Condens. Matter* **2009**, *21*, 335502.
(44) J. Worm Winsal 3.02. http://res-tec.de/tutorial2-01.html.
(45) Walpita, L. M. Solutions for Planar Optical Waveguide Equations by Selecting Zero Elements in a Characteristic Matrix. *J. Opt. Soc. Am. A* **1985**, *2*, 595.
(46) Del Rosso, T.; Sánchez, J. E. H.; Carvalho, R. D. S.; Pandoli, O.; Cremona, M. Accurate and Simultaneous Measurement of Thickness and Refractive Index of Thermally Evaporated Thin

Organic Films by Surface Plasmon Resonance Spectroscopy. *Opt. Express* **2014**, *22*, 18914.
(47) Shalabney, A.; Abdulhalim, I. Electromagnetic Fields Distribution in Multilayer Thin Film Structures and the Origin of Sensitivity Enhancement in Surface Plasmon Resonance Sensors. *Sensors Actuators A Phys.* **2010**, *159*, 24−32.
(48) Shalabney, A.; Abdulhalim, I. Sensitivity-Enhancement Methods for Surface Plasmon Sensors. *Laser Photon. Rev.* **2011**, *5*, 571−606.
(49) Soler, J. M.; Artacho, E.; Gale, J. D.; García, A.; Junquera, J.; Ordejón, P.; Sánchez-Portal, D. The SIESTA Method for Ab Initio Order- N Materials Simulation. *J. Phys.: Condens. Matter* **2002**, *14*, 2745−2779.
(50) Berland, K.; Hyldgaard, P. Exchange Functional That Tests the Robustness of the Plasmon Description of the van Der Waals Density Functional. *Phys. Rev. B* **2014**, *89*, No. 035412.
(51) Pseudopotentials for SIESTA. https://departments.icmab.es/leem/siesta/Pseudopotentials/.
(52) Shtepliuk, I.; Yakimova, R. Interaction of H and Li with Epitaxial Graphene on SiC: A Comparative Analysis by First Principles Study. *Appl. Surf. Sci.* **2021**, *568*, 150988.
(53) Shtepliuk, I.; Ivanov, I. G.; Pliatsikas, N.; Iakimov, T.; Lara-Avila, S.; Kim, K. H.; Sedrine, N. B.; Kubatkin, S. E.; Sarakinos, K.; Yakimova, R. Clustering and Morphology Evolution of Gold on Nanostructured Surfaces of Silicon Carbide: Implications for Catalysis and Sensing. *ACS Appl. Nano Mater.* **2021**, *4*, 1282−1293.
(54) Shtepliuk, I.; Ivanov, I. G.; Pliatsikas, N.; Iakimov, T.; Beshkova, M.; Sarakinos, K.; Yakimova, R. Exploring the Interface Landscape of Noble Metals on Epitaxial Graphene. *Phys. Status Solidi Appl. Mater. Sci.* **2021**, *218*, 2000673.
(55) Shtepliuk, I.; Yakimova, R. Computational Appraisal of Silver Nanocluster Evolution on Epitaxial Graphene: Implications for CO Sensing. *ACS Omega* **2021**, *6*, 24739−24751.
(56) Johnson, P. B.; Christy, R. W. Optical Constants of the Noble Metals. *Phys. Rev. B* **1972**, *6*, 4370−4379.
(57) Biró, L. P.; Lambin, P. Grain Boundaries in Graphene Grown by Chemical Vapor Deposition. *New J. Phys.* **2013**, *15*, No. 035024.
(58) Cançado, L. G.; Jorio, A.; Ferreira, E. H. M.; Stavale, F.; Achete, C. A.; Capaz, R. B.; Moutinho, M. V. O.; Lombardo, A.; Kulmala, T. S.; Ferrari, A. C. Quantifying Defects in Graphene via Raman Spectroscopy at Different Excitation Energies. *Nano Lett.* **2011**, *11*, 3190−3196.
(59) Lupton, E. M.; Achenbach, F.; Weis, J.; Bräuchle, C.; Frank, I. Modified Chemistry of Siloxanes under Tensile Stress: Interaction with Environment. *J. Phys. Chem. B* **2006**, *110*, 14557−14563.
(60) Pallavicini, P.; Dacarro, G.; Galli, M.; Patrini, M. Spectroscopic Evaluation of Surface Functionalization Efficiency in the Preparation of Mercaptopropyltrimethoxysilane Self-Assembled Monolayers on Glass. *J. Colloid Interface Sci.* **2009**, *332*, 432−438.
(61) Zhao, Y.; Xie, Y.; Hui, Y. Y.; Tang, L.; Jie, W.; Jiang, Y.; Xu, L.; Lau, S. P.; Chai, Y. Highly Impermeable and Transparent Graphene as an Ultra-Thin Protection Barrier for Ag Thin Films. *J. Mater. Chem. C* **2013**, *1*, 4956.
(62) Zeng, S.; Sreekanth, K. V.; Shang, J.; Yu, T.; Chen, C.-K.; Yin, F.; Baillargeat, D.; Coquet, P.; Ho, H.-P.; Kabashin, A. V.; Yong, K.-T. Graphene-Gold Metasurface Architectures for Ultrasensitive Plasmonic Biosensing. *Adv. Mater.* **2015**, *27*, 6163−6169.
(63) Bruna, M.; Borini, S. Optical Constants of Graphene Layers in the Visible Range. *Appl. Phys. Lett.* **2009**, *94*, No. 031901.
(64) Weber, J. W.; Calado, V. E.; van de Sanden, M. C. M. Optical Constants of Graphene Measured by Spectroscopic Ellipsometry. *Appl. Phys. Lett.* **2010**, *97*, No. 091904.
(65) Hamada, I.; Otani, M. Comparative van Der Waals Density-Functional Study of Graphene on Metal Surfaces. *Phys. Rev. B* **2010**, *82*, 153412.
(66) Sławińska, J.; Dabrowski, P.; Zasada, I. Doping of Graphene by a Au(111) Substrate: Calculation Strategy within the Local Density Approximation and a Semiempirical van Der Waals Approach. *Phys. Rev. B* **2011**, *83*, 245429.
(67) Hong, G.; Han, Y.; Schutzius, T. M.; Wang, Y.; Pan, Y.; Hu, M.; Jie, J.; Sharma, C. S.; Müller, U.; Poulikakos, D. On the Mechanism of Hydrophilicity of Graphene. *Nano Lett.* **2016**, *16*, 4447−4453.
(68) Kuzmenko, A. B.; van Heumen, E.; Carbone, F.; van der Marel, D. Universal Optical Conductance of Graphite. *Phys. Rev. Lett.* **2008**, *100*, 117401.
(69) Del Rosso, T.; Margulis, W.; Fontana, J.; Carvalho, I. C. S. Plasmonics for the Characterization of Metal Organic Films and Nanoparticles. In *Metal Nanostructures for Photonics*; Elsevier, 2019; pp 223−259.
(70) Shen, H.; Guillot, N.; Rouxel, J.; Lamy de la Chapelle, M.; Toury, T. Optimized Plasmonic Nanostructures for Improved Sensing Activities. *Opt. Express* **2012**, *20*, 21278.
(71) Homola, J.; Koudela, I.; Yee, S. S. Surface Plasmon Resonance Sensors Based on Diffraction Gratings and Prism Couplers: Sensitivity Comparison. *Sensors Actuators B Chem.* **1999**, *54*, 16−24.
(72) Del Rosso, T.; Rey, N. A.; Rosado, T.; Landi, S.; Larrude, D. G.; Romani, E. C.; Junior, F. L. F.; Quinteiro, S. M.; Cremona, M.; Aucelio, R. Q.; Margheri, G.; et al. Synthesis of Oxocarbon-Encapsulated Gold Nanoparticles with Blue-Shifted Localized Surface Plasmon Resonance by Pulsed Laser Ablation in Water with CO 2 Absorbers. *Nanotechnology* **2016**, *27*, 255602.
(73) Del Rosso, T.; Louro, S. R. W.; Deepak, F. L.; Romani, E. C.; Zaman, Q.; Tahir; Pandoli, O.; Cremona, M.; Freire Junior, F. L.; De Beule, P. A. A.; et al. Biocompatible Au@Carbynoid/Pluronic-F127 Nanocomposites Synthesized by Pulsed Laser Ablation Assisted CO2 Recycling. *Appl. Surf. Sci.* **2018**, *441*, 347−355.
(74) Bhavsar, K.; Prabhu, R. Investigations on Sensitivity Enhancement of SPR Biosensor Using Tunable Wavelength and Graphene Layers. *IOP Conf. Ser. Mater. Sci. Eng.* **2019**, *499*, No. 012008.





https://doi.org/10.1021/acs.jpcc.2c02841
*J. Phys. Chem. C* 2022, 126, 13905−13919